DELPHI 97-97 CONF 79
28 July, 1997

Preliminary search for long-lived $\tilde{\tau}$ using the DELPHI detector

Preliminary

DELPHI Collaboration

C. Lacasta[1] , C. García[2], R. Alemany[2] , F. Cavallo[3], F.L. Navarria[3]

Abstract

A search for long-lived scalar leptons in e^+e^- interactions at centre-of-mass energies of 130–136,161 and 172 GeV has been carried out using the data collected by the DELPHI experiment at LEP, in the frame of "low-scale supersymmetry breaking" models. In these models the LSP is the gravitino ($\tilde{G}$), while the NLSP could be a charged scalar lepton like the $\tilde{\tau}$. The search is based on secondary vertex reconstruction when the decay takes place inside the central tracking detectors, while, for shorter lifetimes, two different methods based on track impact parameter have been developed. No indication of the existence of these particles has been found in the data and upper limits on the $\tilde{\tau}$ production cross-section have been set. As a result the present analysis excludes $\tilde{\tau_R}$ masses below 55 GeV/c^2 for 2.5 eV/c^2 $< m_{\tilde{G}} <$95 eV/c^2 and $\tilde{\tau_R}$ masses below 65 GeV/c^2 for 40 eV/c^2 $< m_{\tilde{G}} <$80 eV/c^2 at 95% CL. The combination of these results with those of the search for stable heavy charged particles already published by the DELPHI Collaboration and with the conventional MSSM $\tilde{\tau}$ search completely excludes $\tilde{\tau_R}$ masses in the range 45 GeV/c^2 to 55.5 GeV/c^2.

Paper submitted to the LP'97 Conference
Hamburg, July 28 - August 1st

[1]CERN, CH 1211 Meyrin, Geneve (Switzerland).
[2]IFIC, Avda Dr. Molliner 50, E-46100 Burjasot, Valencia (Spain).
[3]INFN, sez. di Bologna, Viale Berti Pichat 6/2, I-40126 Bologna

1 Introduction

If supersymmetry at the electro-weak scale is established, one of the most important questions to address experimentally is the scale and mechanism of supersymmetry breaking. It is often assumed that the messengers of supersymmetry breaking are gravitational strength interactions and the breaking scale in a hidden sector is of order 10^{11} GeV. An alternative possibility is that supersymmetry is broken at some low scale (between the the Plank and the electro-weak scale), and that the ordinary gauge interaction acts as the messenger of supersymmetry breaking [1, 2]. In this case, the gravitino is naturally the lightest supersymmetric particle (LSP) and the lightest standard model superpartner is the next-to-lightest supersymmetric particle (NLSP).

In local supersymmetry, the Goldstino ($\tilde{G}$) becomes the longitudinal component of the gravitino, giving a gravitino mass of [4]:

$$m_{\tilde{G}} = \frac{F}{\sqrt{3}M_p} \simeq 2.5 \left(\frac{\sqrt{F}}{100\,\mathrm{TeV}}\right)^2 \quad eV \tag{1}$$

where M_p is the Plank mass and $\sqrt{F}$ is the supersymmetry breaking scale. The Goldstino couples to ordinary matter through interactions suppressed only by the supersymmetry breaking scale [5]. Then, the lightest standard model superpartner is unstable and decays to its partner plus the Goldstino. For $\sqrt{F}$ between roughly 100-1000 TeV, this decay can take place within the detector leading to signatures for supersymmetry which are distinct from the conventional minimal supersymmetric standard model (MSSM) as described in [3]. This range of $\sqrt{F}$ is in fact consistent with astrophysical and cosmological considerations [4].

Since the Goldstino couplings are suppressed compared to electro-weak and strong interactions, the decay rate into a Goldstino is only relevant for the lightest standard model superpartner and the pair-production of supersymmetric particles at high energy colliders therefore takes place through standard model couplings. Supersymmetric particles eventually decay to the NLSP, which, in turn, decays into its partner and a Goldstino. The specific signatures of such decays depend crucially on the model-dependent quantum numbers and composition of the lightest standard model superpartner.

Although most of the attention has been focused on the case in which the neutralino is the NLSP, it is equally possible that the NLSP is a charged lepton and, in particular, a $\tilde{\tau}$. The number of $5+\bar{5}$ generations of the gauge mediate messenger, over most of the parameter space, determine the NLSP [6]. For example, for one generation of $5+\bar{5}$ the neutralino tends to be the NLSP, while for two or more generations the balance tips towards right handed leptons.

If the NLSP is a slepton ($\tilde{l}$), its decay width is given by the two-body equation [7]:

$$\Gamma(\tilde{l} \to l + \tilde{G}) = \frac{m_{\tilde{l}}^5}{48\pi M_p^2 m_{\tilde{G}}^2} \tag{2}$$

where SM fermions have been taken as massless. The mean decay length obtained from equation (2):

$$L = 1.76 \times 10^{-3} (E^2/m_{\tilde{l}}^2 - 1)^{\frac{1}{2}} \left(\frac{m_{\tilde{l}}}{100\,GeV}\right)^{-5} \left(\frac{m_{\tilde{G}}}{1\,eV}\right)^2 \quad cm \tag{3}$$

depends strongly on the slepton mass ($m_{\tilde{l}}$) and on the gravitino mass ($m_{\tilde{G}}$) as shown in Figure 1. If $m_{\tilde{l}} \sim 60$ GeV/c^2 and $m_{\tilde{G}}$ between ~ 6.5 to 80 eV, mean decay lengths from 1 to 150 cm are obtained. Therefore, very distinctive signatures can be observed for low scale supersymmetry breaking depending on $m_{\tilde{l}}$ and $m_{\tilde{G}}$.

This paper describes a search for long-lived, right-handed $\tilde{\tau}$'s, with the $\tilde{\tau}$ decaying into a gravitino and a τ within the detector volume. The signature of such events would be a charged track with a kink or a secondary decay vertex when the $\tilde{\tau}$ decays inside the tracking devices (Analysis 1). If the decay length is too short (small $m_{\tilde{G}}$) to allow for the reconstruction of the $\tilde{\tau}$ track, only the decay products of the τ will be seen in the detector, and the search has to be based on the measurement of track impact parameters (Analyses 2 and 3). At one extreme, if the decay takes place outside the tracking devices (large $m_{\tilde{G}}$), the signature will be that of a stable heavy charged particle (Analysis 0) already searched for in DELPHI [8]. At the other extreme, if the decay length is too short to be detected, the final state will be identical to that of the MSSM $\tilde{\tau}$ in the limit of vanishing neutralino mass ($m_{\tilde{\chi}_1^0} \to 0$) (Analysis 4). A combination of these searches was used to investigate the widest possible range of $\tilde{G}$ masses.

The experimental procedure and the event selection are described in section 2, while the combined results are presented in section 3.

2 Experimental procedure and event sample

The analysis is based on data collected by DELPHI during 1995 and 1996 at centre-of-mass energies from 130 to 136 GeV in 1995, 161 GeV and 172 GeV in 1996. The total integrated luminosities for the three periods correspond to 5.9 pb^{-1}, 9.8 pb^{-1} and 9.9 pb^{-1}, respectively. A detailed description of the DELPHI detector can be found in [9] and its performance in [10]. This analysis was mainly based on the following DELPHI tracking devices:

- the Micro Vertex Detector (VD), which consists of three coaxial cylindrical layers of silicon strips detectors at average radii of 6.3, 9.0 and 10.9 cm with acceptance in the polar angle θ defined by $25° \leq \theta \leq 155°$.
- the Inner Detector (ID), which is formed by two different chambers covering the radial region between 12 cm and 23 cm and polar angles between 15° and 165°.
- the Time Projection Chamber (TPC), which provides up to 16 space points per track at radii of 40 to 110 cm between polar angles of 20° and 160°.

In order to compute the detection efficiency for the signal a total of $\sim$80,000 events (subdivided in about 48 different samples) with centre-of-mass energies of 133, 161 and 172 GeV, $\tilde{\tau}$ mean decay length ranging from 0.25 cm to 1000 cm and $\tilde{\tau}$ masses from 45 to 80 GeV/c^2 were generated and passed through the full DELPHI detector simulation package [11].

2.1 Data preselection

A common event preselection was used for Analyses 1 and 2. This preselection is based on a set of rather loose general requirements imposed to real and simulated data in order to suppress the low energy background (beam gas, beam wall, etc) and to reject the main standard model backgrounds (mainly $\gamma\gamma$ events). The adopted cuts are the following:

1. charged multiplicity between 2 and 10,
2. less than 4 tracks reconstructed by the VD only,
3. visible energy above 10 GeV,
4. transverse momentum, with respect to the beam axis, greater than 5 GeV/c,
5. energy measured in the very forward calorimeters below 10 GeV.

Cut 1 rejected hadronic events (upper cut) and low energy background (lower cut), cuts 2 and 3 reduced low energy background and some $\gamma\gamma$ interactions, while cuts 4 and 5 were adopted to further reduce the $\gamma\gamma$ contamination. The same set of requirements was adopted for all centre-of-mass energies.

As an example, Figure 2 shows the event charged multiplicity, visible energy, transverse momentum and forward energy for 60 GeV/c^2 $\tilde{\tau}$ with a mean decay length of 50 cm. For comparison, Figure 2 also shows the full data sample, while a simulated background sample of $\gamma\gamma \rightarrow \tau\tau$ events is shown in Figure 3. About 99% of these background events were rejected by the preselection cuts. In the data, 4.6% of the initial sample survived the preselection.

No quality requirements were imposed on the reconstructed tracks at this stage since all the information had to be used for the vertex reconstruction.

In order to reconstruct secondary vertices, the tracks were first grouped into clusters according to their first measured point (or starting point, SP). The iterative procedure [12] applied to the data worked as follows. The pair of tracks with the smallest separation at their respective starting points was first selected. If this separation was smaller than 2 cm, the tracks were grouped to form a cluster whose starting point was defined as the average of the first measured points of the tracks. The two tracks were then replaced by this cluster, which was subsequently treated as a pseudo-track. The process was then repeated until all charged particle tracks or pseudo-tracks were grouped into clusters.

2.2 Analysis 1: search for decay vertices

After the data preselection, the analysis tried to exploit the peculiarity of the decay $\tilde{\tau} \rightarrow \tau\tilde{G}$ topology. For decay lengths around 50 cm, the event topology is namely one or two tracks coming from the interaction point and at least one of them with either a secondary vertex or a kink. Figure 4 shows a typical event where both $\tilde{\tau}$ decay inside the detector.

The events in which more than 6 tracks were not grouped into clusters or no cluster was found were rejected. As an example, in the event shown in Figure 4, four clusters were reconstructed, each of them having only one track. Two of the clusters contain the $\tilde{\tau}$ tracks while the other two the decay product of each τ.

Among all reconstructed clusters, single-track clusters were considered as candidates of $\tilde{\tau}$ track (track coming from the interaction point) if:

- the distance of the first measured point ($R_{sp}^{\tilde{\tau}}$) to the beam spot in the plane perpendicular to the beam axis (XY plane) was smaller than 10 cm,
- its momentum was greater than 2 GeV/c,
- $|\cos\theta_{trk}| < 0.8$, where θ is the polar angle of the tracks with respect to the beam axis,
- and the impact parameter of the track along the beam axis and in the plane perpendicular to it was smaller than 10 and 5 cm, respectively.

For each $\tilde{\tau}$ candidate (or single-track cluster fulfilling the above conditions), a search was made for a second cluster for which the distance of its starting point to the beam spot in the XY plane was larger than $R_{sp}^{\tilde{\tau}}$ and the angular separation between the directions defined by the starting points and the beam spot in the XY plane was smaller than 90°. This second cluster was supposed to be formed by the decay products of the τ coming from the $\tilde{\tau} \to \tau\tilde{G}$ decay. Therefore, the $\tilde{\tau}$ candidate and the τ cluster must define a secondary vertex. If the τ cluster included more than one track, only the track with the largest momentum was used to search for a decay vertex or a kink (crossing point with the $\tilde{\tau}$ track).

The tracks were then parametrised with respect to their *perigee*[13], so that the particle trajectories could be written as:

$$\begin{aligned} x &= x_C + (1/\rho)\sin(\phi + \rho L) \\ y &= y_C - (1/\rho)\cos(\phi + \rho L) \\ z &= z_p + L\cot\theta \end{aligned} \tag{4}$$

where x_C and y_C were the coordinates of the centre of the track circumference in the XY plane, $1/\rho$ its radius, z_p was the *perigee* coordinate along the beam axis and ϕ and θ were the azimuthal and polar angles, respectively, of the track at the *perigee*. L was the distance in the XY projection to the *perigee* along the track.

Using eqn.(4) the point of closest approach between the candidate $\tilde{\tau}$ track and the selected track from the τ cluster was calculated. Figure 4 illustrates the reconstruction of a vertex with all the parameters used in the selection. The following conditions were required to define a good crossing point:

- the minimum distance between the tracks had to be smaller than 1 mm on the XY plane,
- the τ daughter track must start after the starting point of the $\tilde{\tau}$ track ($R_{sp}^{\tau} > R_{sp}^{\tilde{\tau}}$),
- the crossing point must be close to the end point of the $\tilde{\tau}$ track and to the start point of the τ daughter, then:

$$\begin{array}{rcccl} -10\,cm & < & (R_{cross} - R_{end}^{\tilde{\tau}}) & < & 25\,cm \\ -25\,cm & < & (R_{cross} - R_{sp}^{\tau}) & < & 10\,cm \end{array}$$

  where $R_{end}^{\tilde{\tau}}$, R_{cross} and R_{sp}^{τ} were the distance of the end point of the $\tilde{\tau}$ track, the crossing point of the tracks and the starting point of the τ daughter track from the beam spot on the XY plane.

The distributions of the geometrical parameter used in the vertex reconstruction in simulated data are shown in Figure 5. Fake secondary vertices could be produced by particles interacting with the detector material or radiating photons. In these cases the particle trajectory may be reconstructed in two separate track segments. To eliminate this kind of processes, additional requirements had to be imposed:

- any hadronic interaction, reconstructed by the package MAMMOTH[14], must be outside of a 5° cone from the kink direction (R_{cross} direction), to reject hadronic interactions in the detector walls,
- when the τ cluster had only one track, no neutral particle had to be reconstructed in a 1° cone around the direction defined by the difference between the $\tilde{\tau}$ momentum and the momentum of the τ daughter, to reject photon radiation,
- the angle between the momenta of the tracks used to define a vertex, calculated in the crossing point, must be larger than 1° to reject segmented tracks.

If no pair of tracks were found to fulfil the previous conditions, the event was rejected. Once all the vertices were reconstructed, the event multiplicity had to be compatible with that of the $\tilde{\tau} \to \tilde{G}\tau$ decay to reject any remaining low energy background. Therefore, the events were divided in hemispheres using the vertex direction. The event was selected if the multiplicity of the hemisphere containing the vertex was lower than 6 and between one and two in the opposite hemisphere.

Mean Decay Length 50 cm		
Energy (GeV)	$m_{\tilde{l}}$ (GeV)	ε (%)
172	50	62.9
	60	62.1
	70	58.8
	80	52.9
	85	42.1
161	50	61.6
	55	62.5
	60	59.8
	70	55.5
	80	35.8
133	45	60.0
	50	60.2
	55	56.3
	60	58.9
	65	46.4

Table 1: Efficiency of the impact parameter search for different $\tilde{\tau}$ masses and centre-of-mass energies at 50 cm mean decay length.

$m_{\tilde{l}} = 60$ GeV$/c^2$				
Decay Length (cm)	ε_2 (%)	ε_1 (%)	ε_0 (%)	ε_{012} (%)
1000	0.0	12.2	30.2	40.5
500	0.0	23.0	24.2	41.6
200	0.0	41.7	12.4	48.9
100	0.8	52.5	4.8	55.6
50	4.2	62.1	0.6	66.5
20	6.6	47.6	0.0	54.2
10	13.4	29.0	0.0	42.4
5	26.0	8.1	0.0	34.1
2	33.5	0.2	0.0	33.7
1	32.9	0.1	0.0	33.0
0.5	25.2	0.1	0.0	25.3
0.25	14.0	0.0	0.0	14.0

Table 2: Efficiency of the large impact parameter search (ε_2), vertex search (ε_1), heavy lepton search (ε_0) and combined efficiency (ε_{012}) for 60 GeV $\tilde{\tau}$ at a centre-of-mass energy of 172 GeV.

The efficiency for the different decay lengths, $\tilde{\tau}$ masses and centre-of-mass energies were calculated by applying the above selections to the simulated signal samples. Table 1 shows the efficiencies for different $\tilde{\tau}$ masses and centre-of-mass energies for a fixed decay length (50 cm). The shape of the efficiency distribution is independent of the $\tilde{\tau}$ mass and of the centre-of-mass energy, but it scales down near the kinematic threshold. The loss of efficiency near the threshold is due to the fact that the $\tilde{\tau}$ boost and the kink reconstruction efficiency decrease when the angles between the $\tilde{\tau}$ and the τ products increase. Table 2 shows the efficiency (ε_1) obtained for a 60 GeV$/c^2$ $\tilde{\tau}$ at a centre-of-mass energy of 172 GeV and mean decay lengths from 0.4 mm to 1000 cm. Figure 6 shows the efficiency of the vertex reconstruction as a function of the distance in the XY plane to the beam spot of the decay length (R). The vertex reconstruction was sensitive to decay radii, R, between 15 cm and 90 cm, since the VD and the ID were needed to reconstruct the $\tilde{\tau}$ track, with an efficiency of $\sim$75%. When the $\tilde{\tau}$ decays around the external edge of the TPC, the efficiency drops to zero. That procedure yields a selection efficiency of about 94% inside the sensitive region, to be multiplied by the fraction of $\tilde{\tau}$ decaying within this volume, which for a mean decay length of 50 cm is about 65%. The trigger efficiency was also studied by simulating the DELPHI trigger response to the event selected by the vertex search and was found to be about 99%.

No candidate events with secondary vertices or kinks were found in the real data sample.

2.3 Analysis 2: large impact parameter search

To investigate the possibility of smaller gravitino masses and, consequently, shorter $\tilde{\tau}$ decay lengths, the previous search was complemented with a different analysis, based on the measurement of track impact parameters. This analysis was optimised for $\tilde{\tau}$ decay lengths in the range between 0.25 cm and 10 cm from the interaction point. In this case the $\tilde{\tau}$ track is not reconstructed and only the τ decay products are detected. Thus the signature for this topology is the presence of tracks with large impact parameter and large acolinearity (figures 7 and 8).

Cosmic rays and badly reconstructed events could have tracks with large impact parameter and fake the presence of signal events, however the two track segments in a cosmic event usually have impact parameters of the same order and opposite sign (see Figure 7), while the acolinearity of events with bad reconstructed tracks is normally small.

This impact parameter search was only applied to those events which were accepted by the preselection cuts described in section 2.1 and rejected by Analysis 1 of section 2.2.

The events were then accepted as candidates for the impact parameter search (Analysis 2) if:

- there were two single-track clusters in the event, i.e. two tracks with momentum larger than 1.5 GeV/c and the distance between starting points larger than 2 cm; if a third cluster was found, it had to contain only a track with length smaller than 20 cm; only the first two clusters were then consider in the analysis;
- at least one of the tracks had to start at less than 12 cm;
- both tracks had to be reconstructed in the TPC, in order to guarantee a good track fit;
- at least one of the tracks had an impact parameter in the transverse plane to the beam axis larger than 0.2 cm to remove standard events;
- the ratio of the impact parameters of the two tracks was smaller than -1.5 and larger than -0.5, to reject cosmic rays;
- the acolinearity between the two tracks must be larger than 10°.

These cuts were determined by studying background events taken from simulated samples of standard model processes and real samples of cosmic data.

The efficiencies were derived for the different $\tilde{\tau}$ masses, mean decay lengths and centre-of-mass energies by applying the same selection to the simulated signal events. Table 2 and Figure 10 show the efficiency of the large impact parameter search (ε_2) for a 60 GeV/c^2 $\tilde{\tau}$ at a 172 GeV centre-of-mass energy. The efficiency turned out to be 33.5% for a mean decay length of 2 cm, decreasing very fast for lower decay lengths due to the cut on the minimum impact parameter. For longer decay lengths the efficiency decreased smoothly due to the request on the maximum number of tracks because in this situation the $\tilde{\tau}$ track could be reconstructed. No dependence on the $\tilde{\tau}$ mass has been observed in the signal efficiency.

No events in the real data sample were selected with the above criteria. Summing up all background contributions for Analyses 1 and 2, 0.6 events were expected in total, 0.4 for Analysis 1 deu to $\gamma\gamma \to \tau\tau$ and $Z\gamma \to \tau\tau\,, ee$ and 0.2 for Analysis 2 deu to $Z\gamma \to ee$.

2.4 Analysis 3: small impact parameter search

For shorter $\tilde{\tau}$ lifetimes, corresponding to decay lengths below 2.5 mm, a third analysis was developed, though still based on impact parameter measurement. In this case the background from standard model processes becomes larger, so a tighter set of preselection cuts were adopted, in order to allow for a looser cut on the impact parameter. In particular, the following set of preliminary cuts were adopted:

1. $2 \leq$ number of charged tracks ≤ 4
2. Visible energy of the event between 8% and 70% of the centre-of-mass energy
3. Transverse missing momentum ≥ 0.03 centre-of-mass energy
4. Polar angle of missing momentum within [30^o,150^o]
5. Energy within the two cones of 30^o around the beam ≤ 0.1 visible energy
6. neutral energy ≤ 0.35 beam energy

After dividing the event into two hemispheres according to the thrust axis and selecting the leading track in each hemisphere, the following requirements were added in order to enhance the signal over the standard model backgrounds:

7. Angle between the leading tracks in the RΦ plane ≤ 3 rad
8. Acolinearity of the two leading tracks $\geq 10^o$
9. Quadratic sum of the two leading track momenta $\sqrt{p_1^2 + p_2^2} \geq 0.06$ beam energy
10. Electromagnetic energy (1) + electromagnetic energy (2) ≤ 0.7 beam energy
11. Quadratic sum of the two leading track impact parameters $\sqrt{i.p._{r1}^2 + i.p._{r2}^2} \geq 0.06$ cm

Cuts 3 to 5 aim at rejecting $\gamma\gamma$ interactions; cuts 6 to 11 suppress the background due to standard $e^+e^- \to f\bar{f}$ processes, cut 11 also reduces standard $e^+e^- \to \tau\tau$ events; finally, cuts 7 and 8 suppress cosmic rays.

The surviving background contamination consists mainly of τ pair-production, via $\gamma\gamma$ interactions or Z/γ exchange. At the centre-of-mass energy of 172 GeV WW events (with at least one W decaying to $\tau\nu_\tau$) also contribute to the background. Summing up all samples corresponding to the different beam energies, 0.83 ± 0.25 events are globally expected in the data from the background simulation, of which 0.12 ± 0.02 are due to WW events at $\sqrt{s} = 172$ GeV.

By applying the above cuts to simulated signal events, the efficiency was found not to depend on the centre-of-mass energy nor on the $\tilde{\tau}$ mass but rather on the $\tilde{\tau}$ decay length alone. The efficiency for the signal is shown in Figure 9 as a function of the $\tilde{\tau}$ decay length for various $\tilde{\tau}$ masses and beam energies.

One event was selected in the data by Analysis 3. However, after a visual scan, this event was unambiguously identified as a cosmic ray. Further details about Analysis 3 can be found in separate note [15].

3 Combined results

Three complementary analyses have been performed to search for long-lived $\tilde{\tau}$'s decaying within the volume of the DELPHI detector. The first method (Analysis 1), based on secondary vertex reconstruction, investigated $\tilde{G}$ masses giving $\tilde{\tau}$ decay lengths larger than $\sim$20 cm. A second one (Analysis 2), based on large impact parameter search, was optimised for lower $\tilde{G}$ masses (from 2 to 20 eV/c^2). A third analysis (Analysis 3), also based on the impact parameter method, was adopted to investigate even smaller $\tilde{G}$ masses and is sensitive to $\tilde{\tau}$ decay lengths shorter than 2.5 mm.

The efficiency as a function of the $\tilde{G}$ mass for a given $m_{\tilde{\tau}}$ was studied using eqn. (3) that relates the mean decay length with the masses and the $\tilde{\tau}$ energy. The loss of efficiency for $\tilde{\tau}$ masses near the kinematic threshold and due to initial state radiation were also considered. In all cases the signal efficiency was found to depend only on the $\tilde{\tau}$ decay length.

The efficiency for Analyses 1 and 2 are described in Table 2 as a function of the mean decay length and in Figures 11 and 10 as a function of the $\tilde{G}$ mass. As the selections are mutually exclusive, no correlation exists between these two analyses and the individual efficiencies could be added.

By combining the results of Analyses 1 and 2 with the search for stable heavy leptons (Analysis 0) described in [8] which investigates the possibility that the $\tilde{\tau}$'s decay outside the DELPHI tracking devices ($R > 200$ cm), with $\tilde{\tau}$ masses from 45 GeV/c^2 to the kinematic threshold. This analysis specially contributed in the region of large $\tilde{G}$ masses (large $\tilde{\tau}$ lifetimes). The individual efficiency of the stable heavy lepton search (ε_0) for 60 GeV/c^2 sleptons at 172 Gev as a function of the decay length is also shown in Table 2. For large $\tilde{\tau}$ masses efficiencies around 80% could be achieved in this case.

Since an event could be selected by the vertex search and by the stable heavy lepton search, the correlation between these analyses was taken into account and a combined efficiency for Analyses 0 and 1 was computed (Figure 12).

Finally, the efficiency obtained by combining Analyses 0, 1 and 2 are shown in Table 2 (ε_{012}) as a function of the mean decay length and in Figure 12 as a function of the $\tilde{G}$ mass.

Upper limits at 95% CL on the production cross-section of $\tilde{\tau}$ were calculated individually for the different centre-of-mass energies (see Figure 14) for Analyses 0, 1 and 2. Lower limits of about 0.6 pb were obtained for $m_{\tilde{G}} >$8 eV at 172 GeV centre-of-mass energy and for $m_{\tilde{G}} >$10 eV at 161 GeV centre-of-mass energy. Due to the lower luminosity at 133 GeV an upper limit on the production cross section of 1 pb was set for $m_{\tilde{G}} >$10 eV.

In case of right-handed $\tilde{\tau}$, the variation of the signal cross-section with the centre-of-mass energy was taken into account to derive the total number of signal events predicted summing up the different samples, so that general limits on $m_{\tilde{\tau}_R}$ could be derived as function of $m_{\tilde{G}}$. Figures 15 and 16 show the exclusion plots obtained from each search. The vertex analysis excludes, at 95% CL, $\tilde{\tau}_R$ masses around 60 GeV/c^2 in the range of intermediate gravitino masses (25 to 100 eV). The heavy stable lepton search is sensitive to gravitino masses over 100 eV, while the impact parameter analysis covers the region of low gravitino masses. The combination of the vertex and impact parameter searches (Analyses 1 and 2) excludes, at 95% CL, $\tilde{\tau}_R$ masses below 55 GeV/c^2 for gravitino masses between 4.5 eV/c^2 and 95 eV/c^2. In addition, $\tilde{\tau}_R$ below 65 GeV/c^2 are also excluded for gravitino masses between 40 and 80 eV/c^2 at 95% CL (see Figure 15).

Because Analysis 3 was developed in an independent way, its efficiency (ε_3) could not be added to the other searches and is shown, separately, in Figure 9. This small impact parameter analysis was used to extend the excluded region in the $m_{\tilde{\tau}}$ versus $m_{\tilde{G}}$ plane down to $m_{\tilde{G}} \sim 1$ eV as described in Figure 16.

As a consequence, by combining this new result with those already discussed, $\tilde{\tau}$ masses of order 55 GeV/c^2 (57 GeV/c^2) can now be excluded for gravitino masses greater than 2.5 eV/c^2 at 95% CL (90% CL).

For even lower $\tilde{G}$ masses the decay length becomes so small that it cannot be detected anymore. However in this case the final state topology becomes identical to that of the MSSM $\tilde{\tau} \rightarrow \tilde{\chi}_1^0 \tau$ decay in the limit of vanishing $\tilde{\chi}_1^0$ masses. For this extreme case (Analysis 4) a dedicated search was performed by the DELPHI Collaboration. The search, described in [16], already excluded masses below 55.5 GeV/c^2 for right-handed $\tilde{\tau}$. As a consequence, the combination of [16] with the searches presented in this paper completely excludes $\tilde{\tau}_R$ masses in the range 45 GeV/c^2 to 55.5 GeV/c^2 independently of the $\tilde{G}$ mass (Figure 17).

References

[1] M. Dine, W Fischler and M. Srednicki, *Nucl. Phys.* **B189** (1981) 575 ; S. Dimopoulos and S. Raby, *Nucl. Phys.* **B192** (1981) 353 ; M. Dine and W. Fischler, *Phys. Lett.* **B110** (1982) 227 ; M. Dine and M. Srednicki, *Nucl. Phys.* **B202** (1982) 238 ; L. Alvarez-Gaumé, M. Claudson and M. Wise, *Nucl. Phys.* **B207** (1982) 96 ; C. Nappi and B. Ovrut, *Phys. Lett.* **B113** (1982) 175 .

[2] M. Dine and W. Fischler, *Nucl. Phys.* **B204** (1982) 346 ; S. Dimopoulos and S. Raby, *Nucl. Phys.* **B219** (1983) 479.

[3] S. Dimopoulos, M Dine, S Raby,S. Thomas and J. D. Wells, hep-ph/9607450.

[4] S. Dimopoulos, M Dine, S Raby and S. Thomas, hep-ph/9601367.

[5] S. Dimopoulos, S. Thomas and D. Wells, hep-ph/9604452.

[6] J. A. Bagger, K. Matchev, D. M. Pierce and R. Zhang, SLAC-PUB-7310.

[7] S. Ambrosanio, G. L. Kane, G. D. Kribs, S. P. Martin and S. Mrenna, hep-ph/9605398.

[8] P. Abreu et al., *Phys. Lett.* **B396** (1997) 315.

[9] P. Aarnio et al., *Nucl. Instr. and Meth.* **303** (1991) 233.

[10] P. Abreu et al.,*Nucl. Instr. and Meth.* **378** (1996) 57.

[11] DELSIM Reference Manual. DELPHI note 89-68 PROG 143, Sep. 1989 (unpublished).

[12] P. Abreu et al., Zeit. Phys. C73 (1997) 243.

[13] P. Billoir and S. Qian,*Nucl. Instr. and Meth.* **311** (1992) 139.

[14] M. Feindt, W. Ohersehulte gen. Beckmann and C. Weiser. DELPHI 96-52 PROG 216.

[15] F. Cavallo, *Search for the decay $\tilde{\tau} \rightarrow \tau\tilde{G}$, in the frame of Minimal Gauge Mediated SUSY Breaking models*, DELPHI internal note, in preparation.

[16] P. Andersson et al., it Search for sfermions at $\sqrt{s}$=161 and 172 GeV, DELPHI contribution to the HEP'97 Conference, Jerusalem, August 19-26 1997.

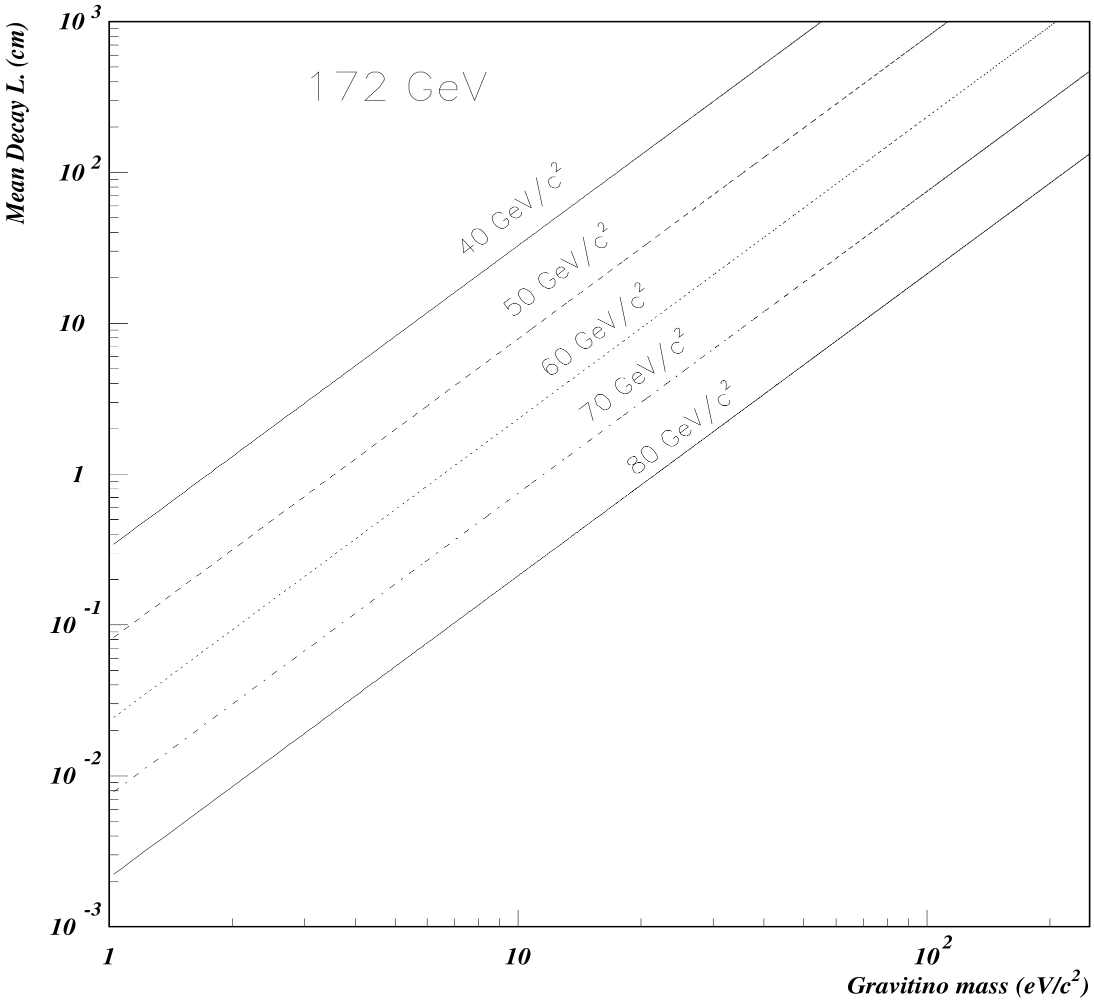

Figure 1: Mean decay length as a function of the gravitino mass for different $\tilde{\tau}$ masses at a centre-of-mass energy of 172 GeV.

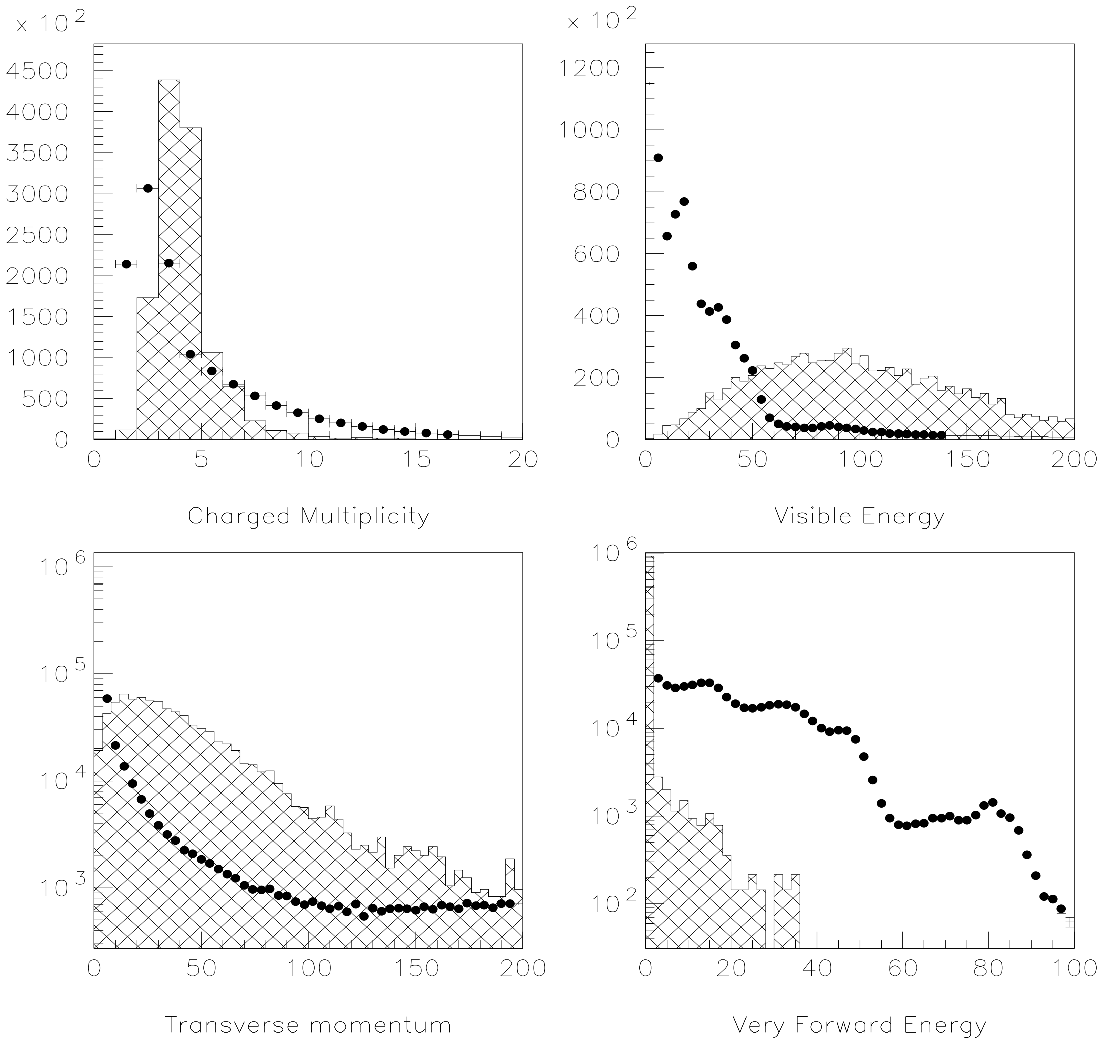

Figure 2: Charged multiplicity, visible energy, transverse momentum and very forward energy distributions. Solid dots represent data while the histogram is the signal simulation for 50 cm mean decay length and centre-of-mass energy of 172 GeV normalised to the data.

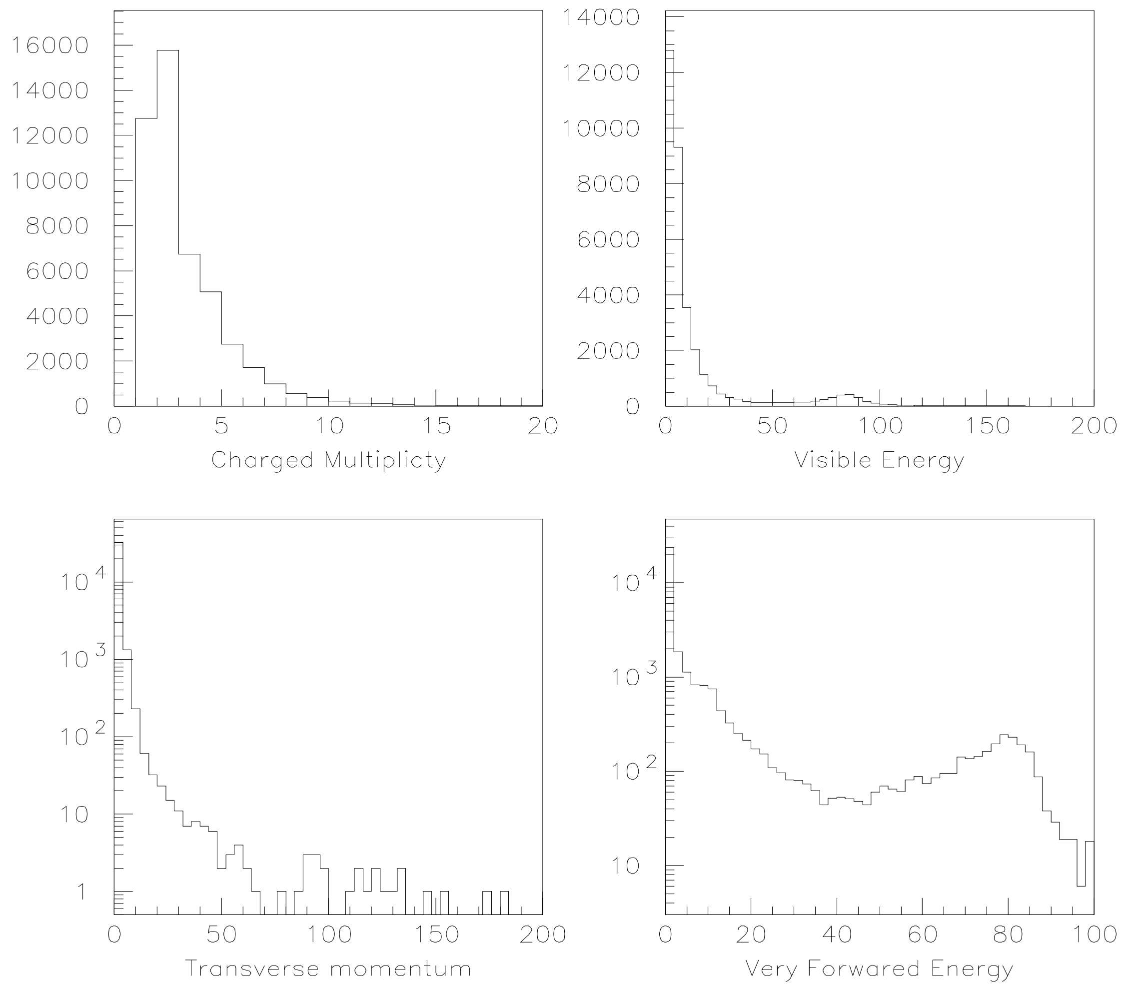

Figure 3: Charge multiplicity, visible energy, transverse momentum and very forward energy distributions for simulated $\gamma\gamma \rightarrow \tau\tau$ background events at 172 GeV centre-of-mass energy.

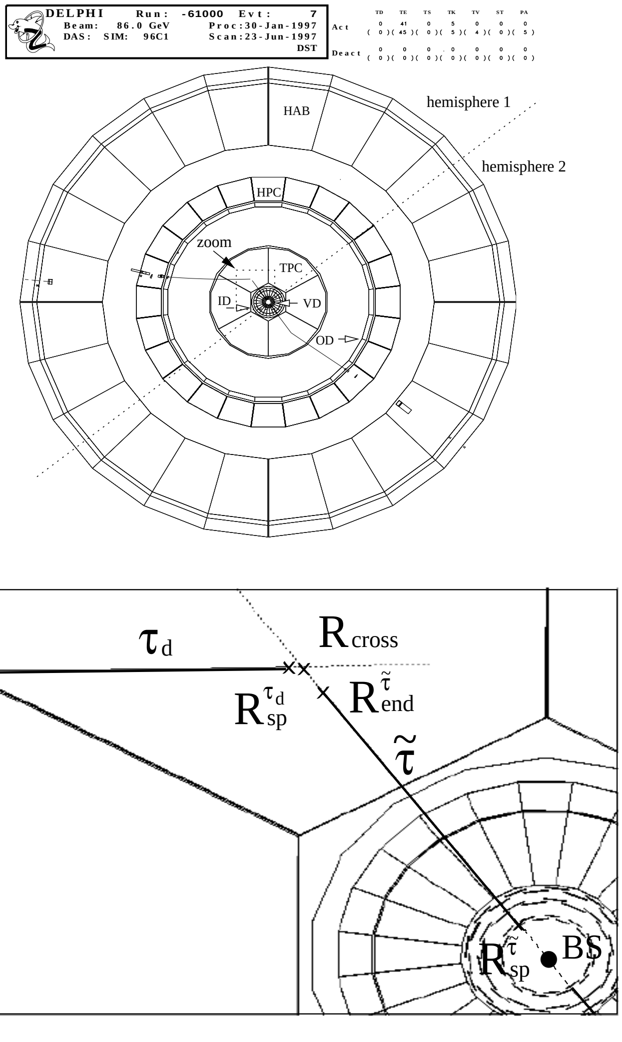

Figure 4: Projection on the XY plane of a signal simulated event, in which both staus decay inside the TPC. One of the decay regions has been zoomed to illustrate the reconstruction of the secondary vertex. The $\tilde{\tau}$ track (labelled with $\tilde{\tau}$) and the track of the τ decay product (labelled with τ_d) are extrapolated (dotted line). The extrapolated tracks define a crossing point (R_{cross}). $R_{sp}^{\tilde{\tau}}$ and $R_{end}^{\tilde{\tau}}$ are the first and last measured points of the $\tilde{\tau}$ track. $R_{sp}^{\tau_d}$ is the first measured point of the selected track among the τ decay product. All the distances are measured with respect to the beam spot (BS).

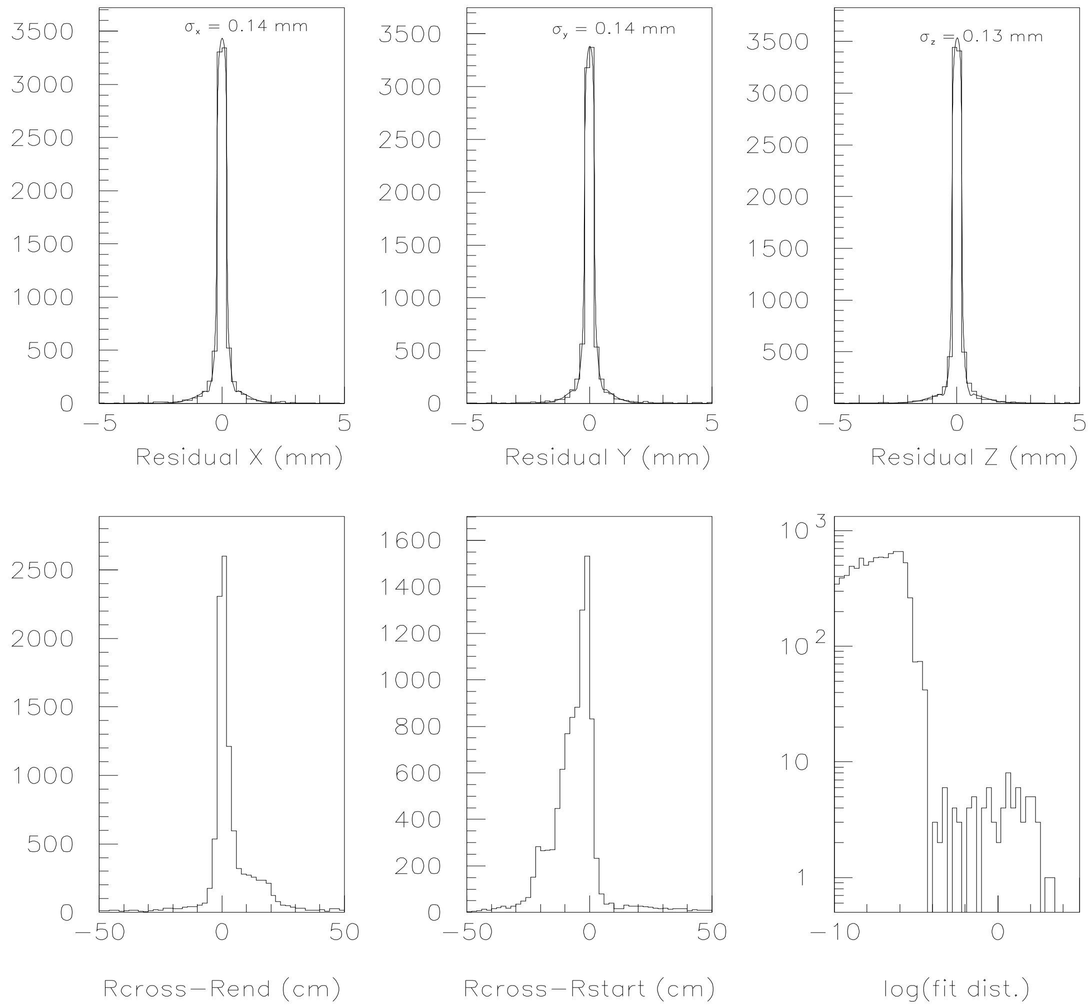

Figure 5: The upper plots show the resolution achieved with the algorithm for the secondary vertex reconstruction in three dimensions, X, Y, and Z. The lower plots show the distance in the XY plane between the crossing point and the end point of the $\tilde{\tau}$ track (left), the distance between the crossing point and the τ daughter track (centre) and the logarithm of the minimum distance between both tracks (right) as found by the algorithm in simulated data.

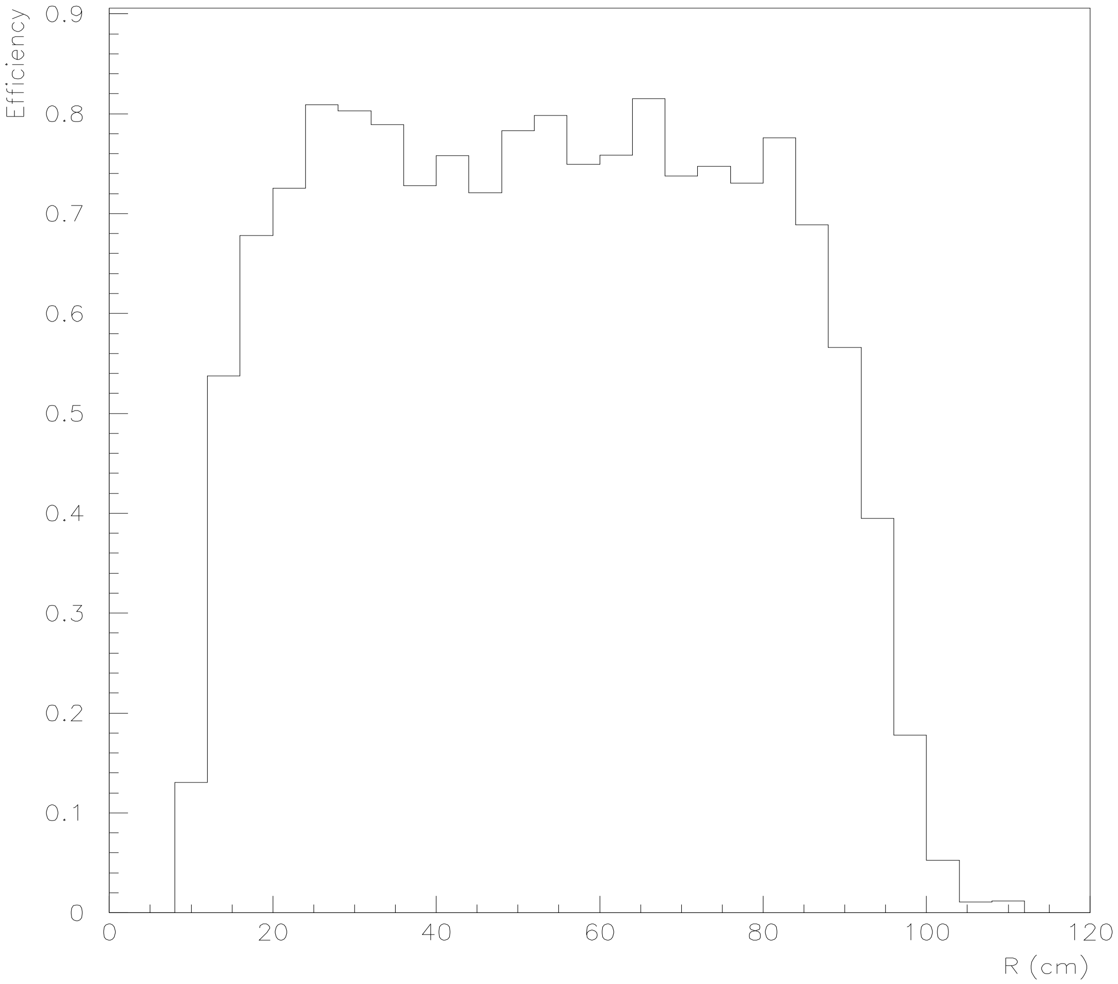

Figure 6: Efficiency for a single vertex reconstruction (Analysis 1) as a function of the radial distance of the decay vertex to the beam spot.

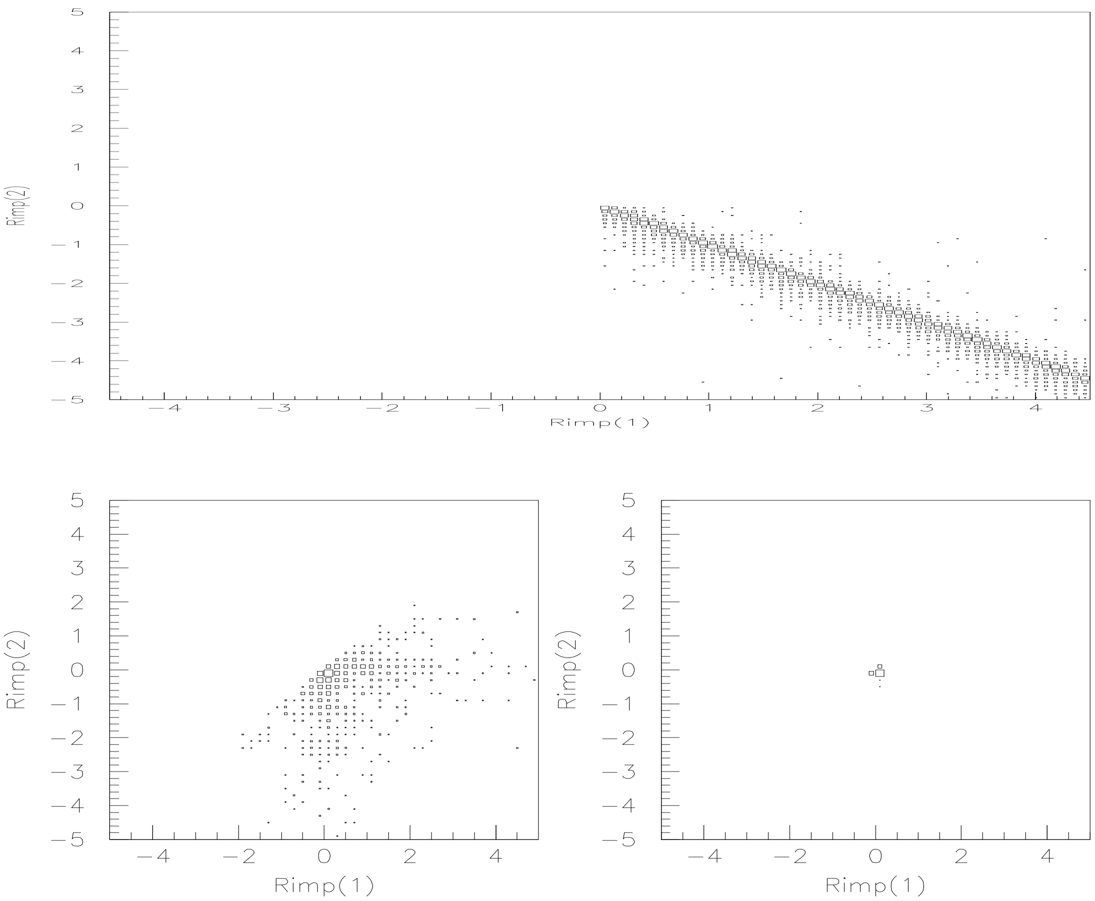

Figure 7: Impact parameter of track 1 versus track 2 in cosmic events (upper plot), for two tracks events of 60 GeV/c^2 $\tilde{\tau}$ with 2 cm mean decay length (left lower plot) and for $\gamma\gamma \to \tau\tau$ events (right lower plot).

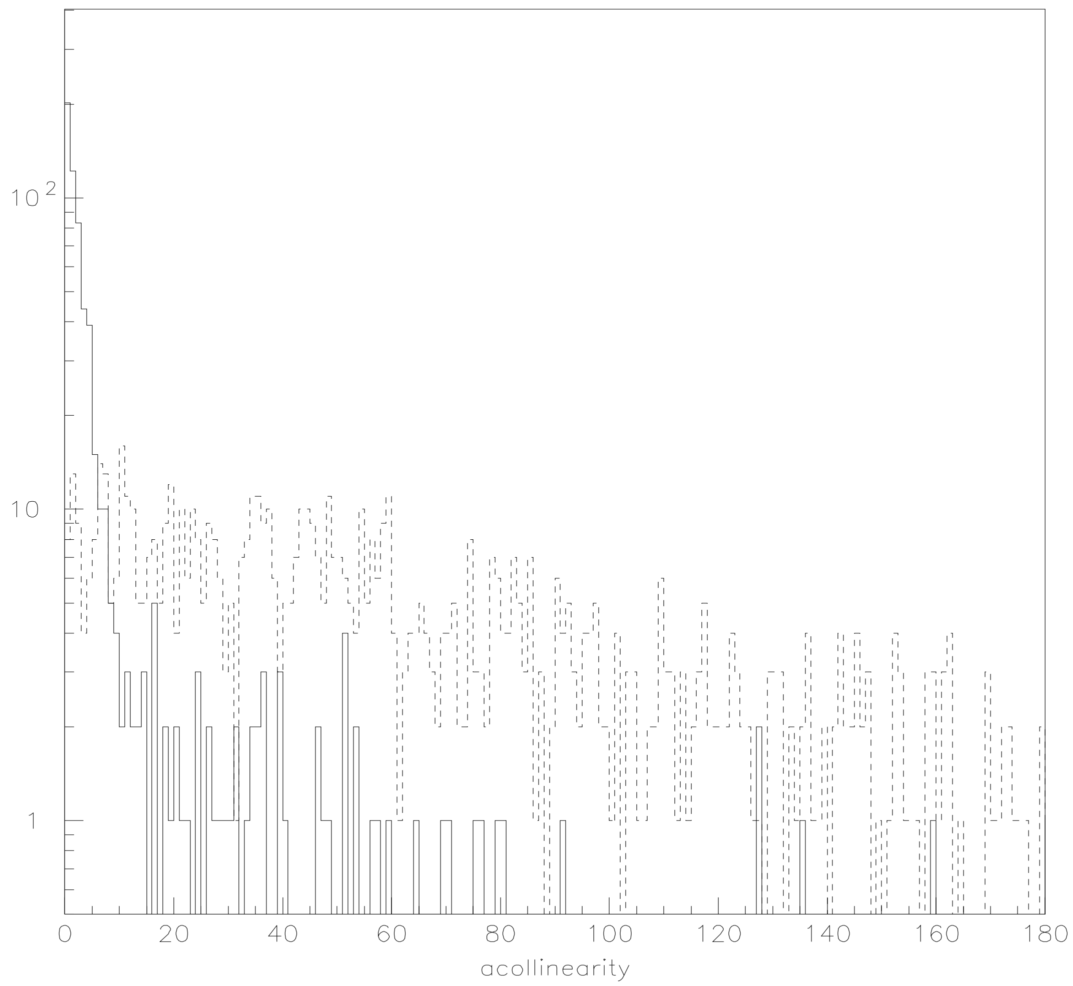

Figure 8: Acolinearity for for 60 GeV/c^2 $\tilde{\tau}$ with a mean decay length of 2 cm (dashed line) and for $\gamma\gamma \rightarrow \tau\tau$ events (solid line).

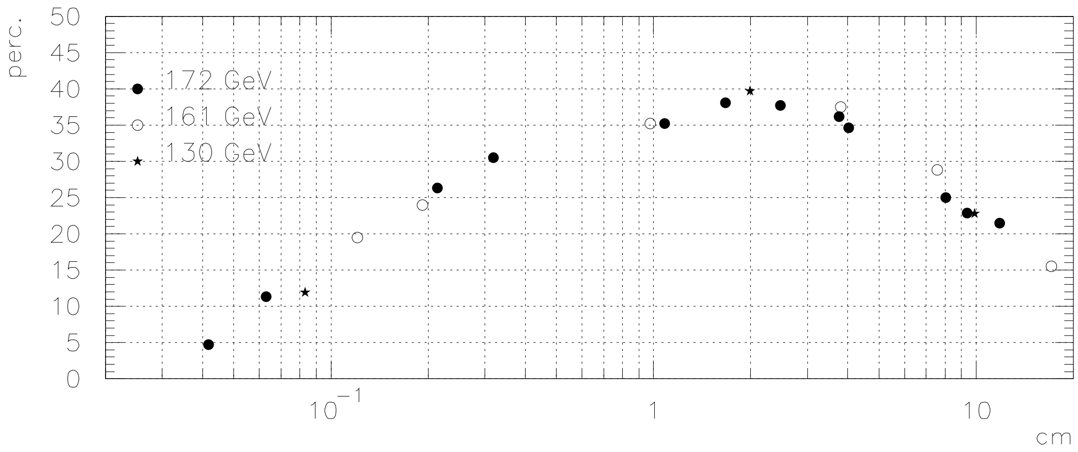

Figure 9: Efficiency of the small impact parameter search (Analysis 3) as a function of the mean decay length.

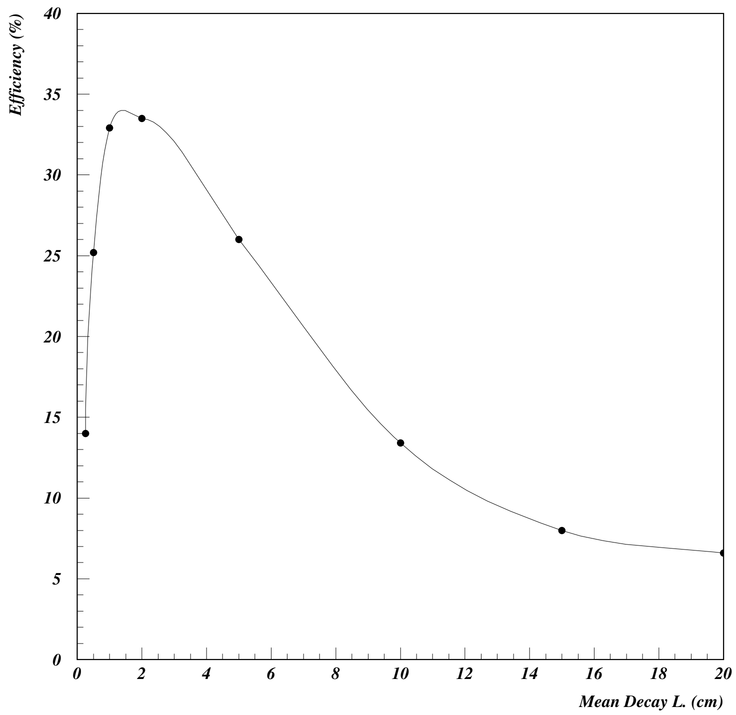

Figure 10: Efficiency of the large impact parameter search (Analysis 2) as a function of the mean decay length.

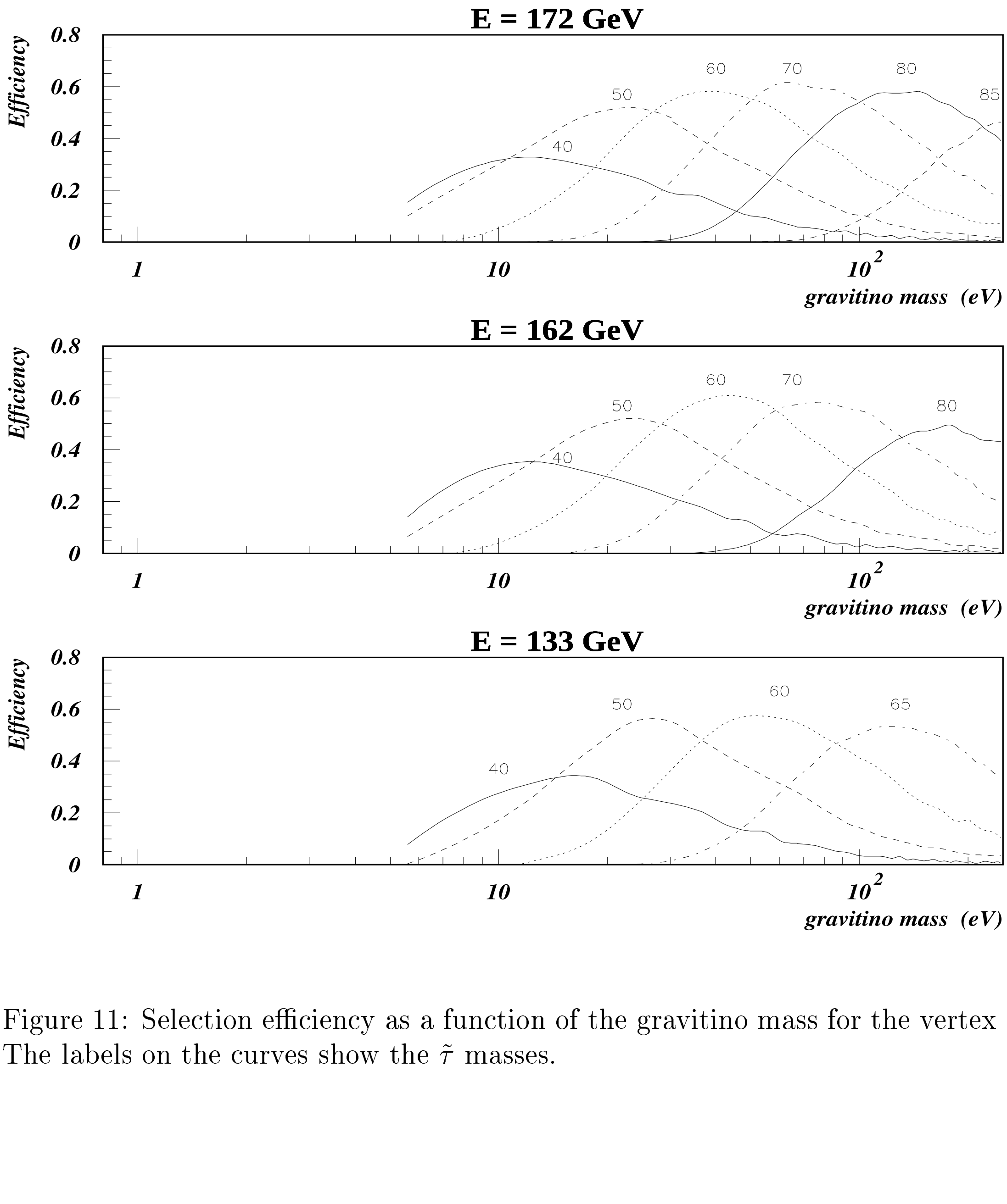

Figure 11: Selection efficiency as a function of the gravitino mass for the vertex analysis. The labels on the curves show the $\tilde{\tau}$ masses.

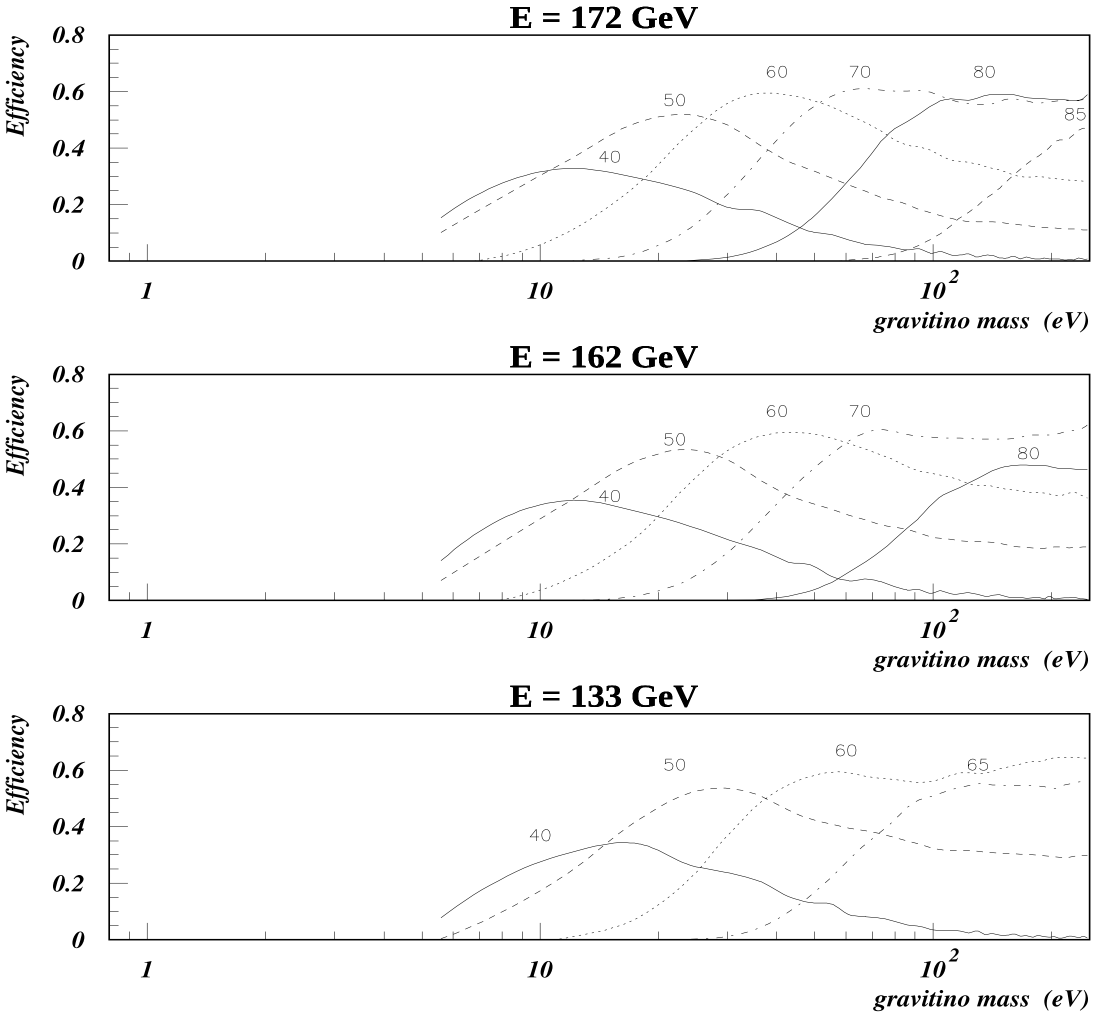

Figure 12: Selection efficiency as a function of the gravitino mass for the vertex analysis combined with the stable heavy lepton search. The labels on the curves show the $\tilde{\tau}$ masses.

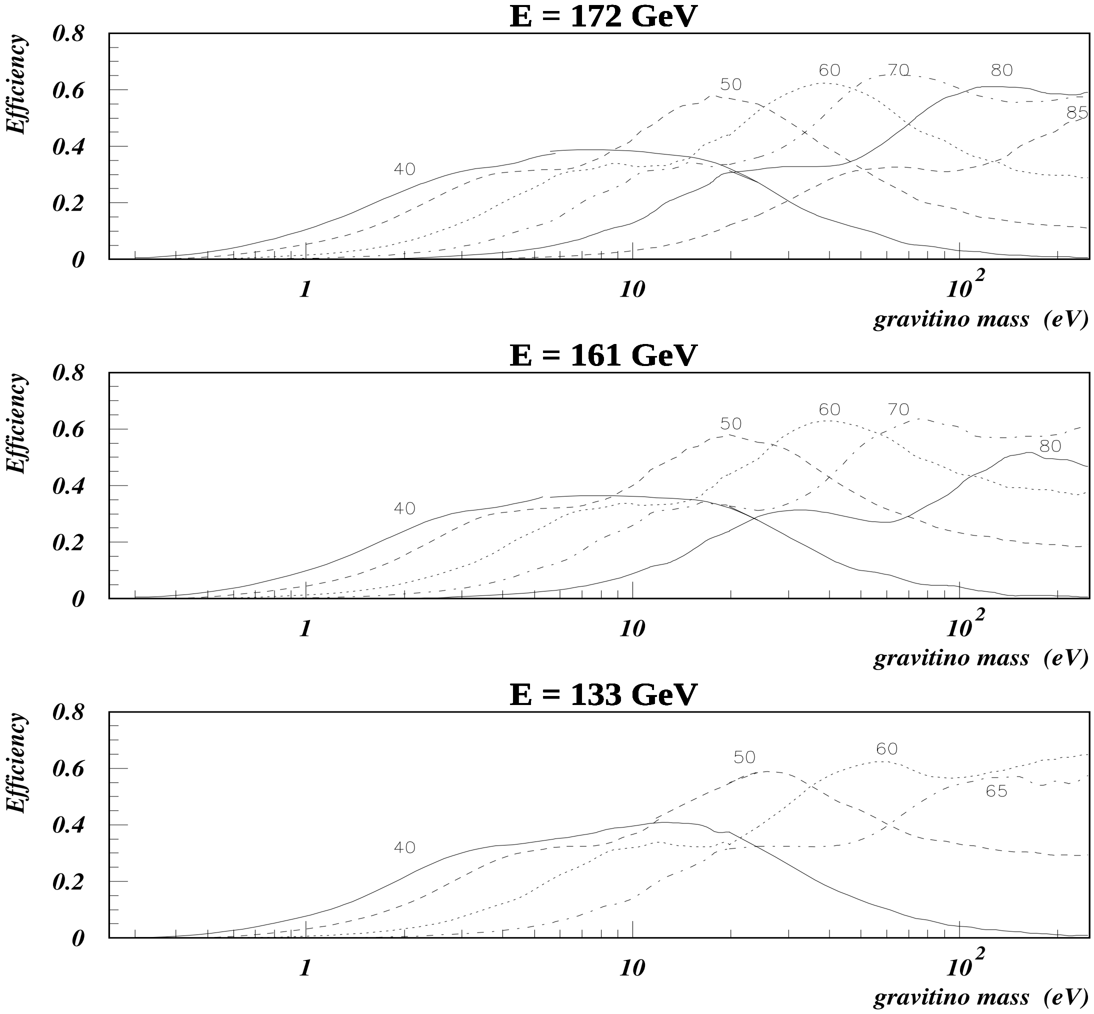

Figure 13: Selection efficiency as a function of the gravitino mass combining the three searches: impact parameter, vertex and heavy lepton search. The labels on the curves show the $\tilde{\tau}$ masses.

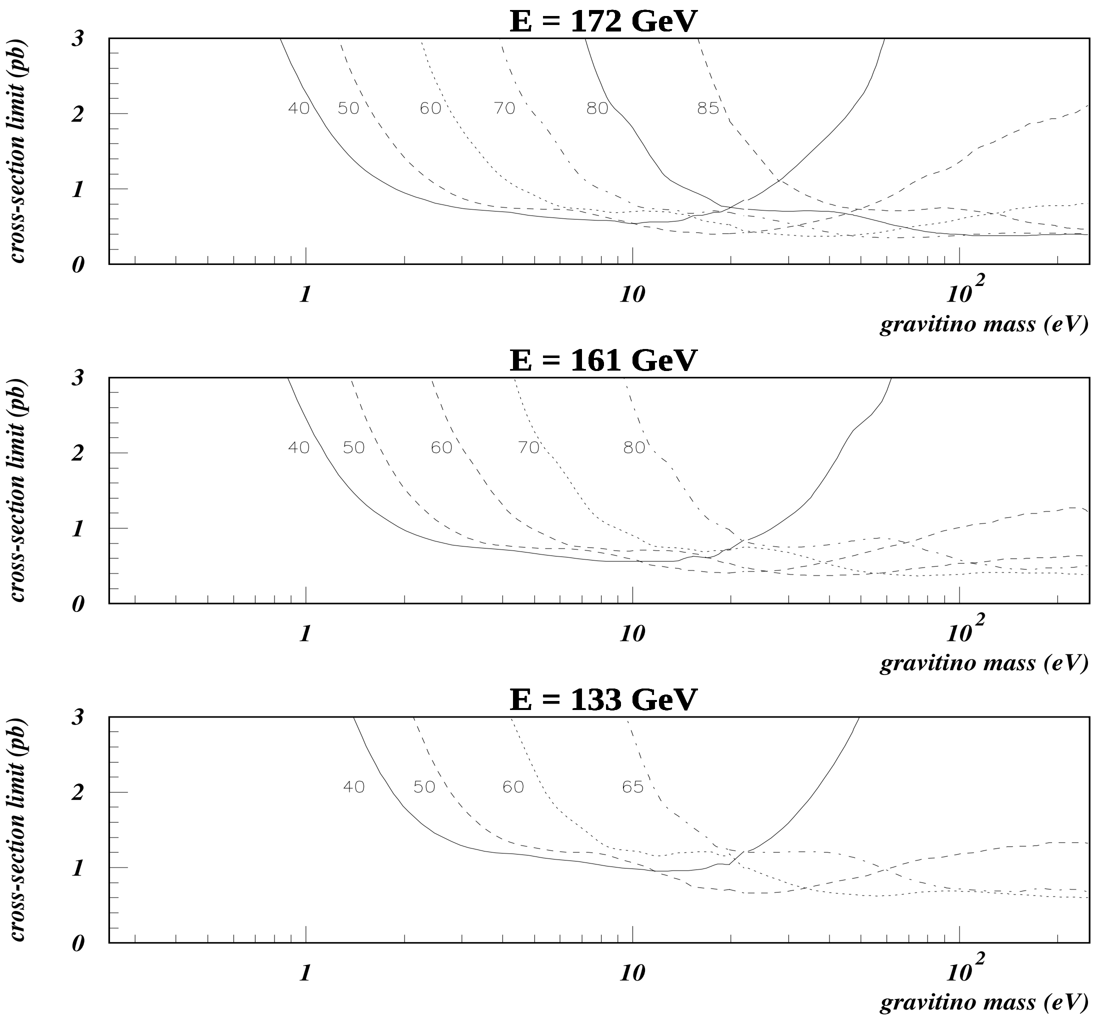

Figure 14: Upper limit for the production cross section at 95% CL set by combining the three analysis: impact parameter, vertex and heavy lepton search. The labels on the curves show the $\tilde{\tau}$ masses.

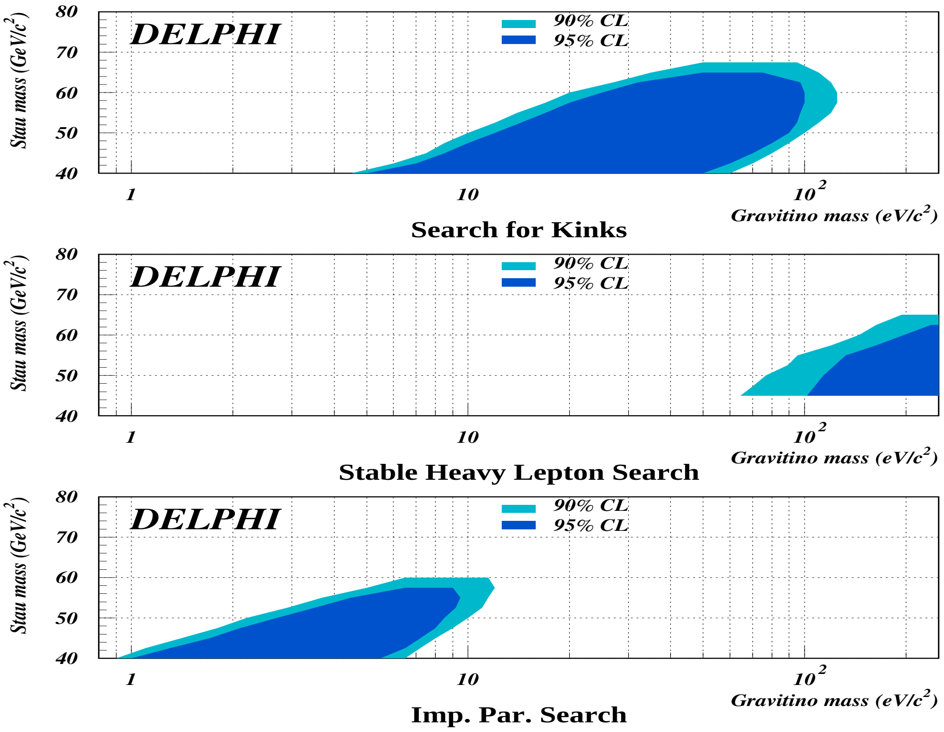

Figure 15: Exclusion plot in the $(m_{\tilde{\tau}},\, m_{\tilde{G}})$ plane at 90% and 95% CL for vertex search, heavy lepton search and impact parameter search.

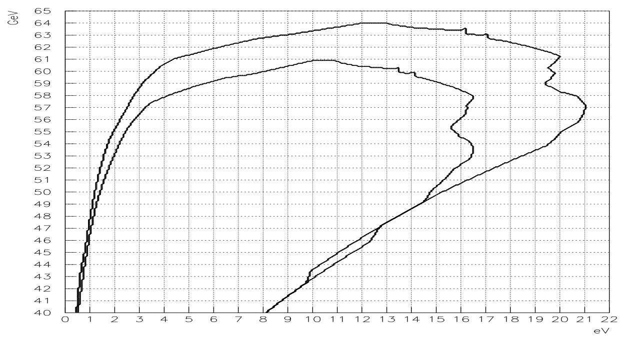

Figure 16: Region in the $(m_{\tilde{\tau}},\, m_{\tilde{G}})$ plane excluded at 90% and 95% CL by Analysis 3 alone.

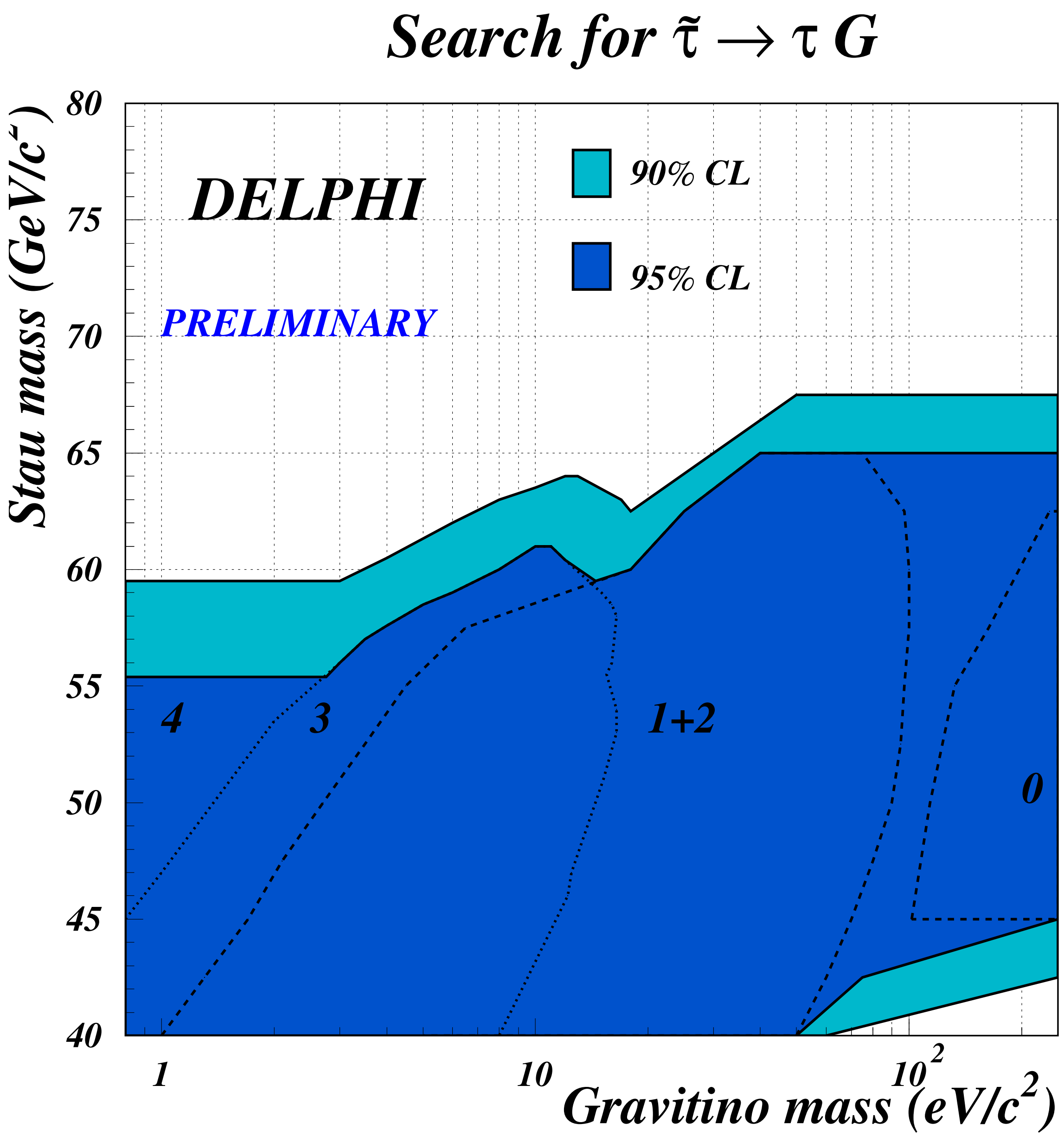

Figure 17: Region in the ($m_{\tilde{\tau}}$, $m_{\tilde{G}}$) plane excluded at 90% and 95% CL by combining Analyses 1, 2 and 3 described in this paper with each other and with the search for heavy stable charged particles (Analysis 0) and MSSM $\tilde{\tau}$ (Analysis 4).